

Observations of Polarized Dust Emission at Far-infrared through Millimeter Wavelengths

John E. Vaillancourt

*Division of Physics, Mathematics, & Astronomy,
California Institute of Technology,
MS 320-47, 1200 E. California Blvd., Pasadena, CA 91125, USA*

Abstract. Interstellar polarization at far-infrared through millimeter wavelengths ($\lambda \sim 0.1 - 1$ mm) is primarily due to thermal emission from dust grains aligned with magnetic fields. This mechanism has led to studies of magnetic fields in a variety of celestial sources, as well as the physical characteristics of the dust grains and their interaction with the field. Observations have covered a diverse array of sources, from entire galaxies to molecular clouds and protostellar disks. Maps have been generated on a wide range of angular scales, from surveys covering large fractions of the sky, down to those with arcsecond spatial resolution. Additionally, the increasing availability of observations at multiple wavelengths in this band allows empirical tests of models of grain alignment and cloud structure. I review some of the recent work in this field, emphasizing comparisons of observations on multiple spatial scales and at multiple wavelengths.

1. Introduction

Dust grains in both diffuse and dense phases of the interstellar medium (ISM) are preferentially aligned by local magnetic fields (e.g., Lazarian 2007). The resulting net polarization is observed across a wide range of wavelengths. At visible and near-infrared wavelengths transmitted starlight has a net polarization due to dichroic extinction from the net alignment of aspherical grains. At longer far-infrared (FIR) and submillimeter (SMM) wavelengths ($\lambda \sim 0.1 - 1$ mm) the polarized radiation is dominated by thermal emission from similar grains. These different polarization mechanisms result in orthogonal polarizations with respect to the aligning field, perpendicular to the field in the case of emission but parallel in the case of absorption and extinction.

Polarimetric observations in the FIR–MM regime cover angular scales ranging from $\sim 1''$ to all-sky. The goal at all scales is to determine the structure of the magnetic field. Previously, observations were limited to ~ 0.3 – a few arcminutes (e.g., Dotson et al. 2000, 2009; Matthews et al. 2008); the limits being set by diffraction at the small end and the size of the largest detector-array field of view (FOV) at the high end. Interferometers are now able to regularly achieve $\sim 1''$ resolution while large beamsizes coupled with efficient scan strategies have made it easier to map regions larger than a single focal plane FOV (e.g., Page et al. 2007; Takahashi et al. 2008).

The increasingly wide range of wavelengths used to observe at each of these scales now allows studies of the polarization spectrum. Just as in the case of total emission, a well sampled spectrum is used to place constraints on mod-

els of molecular cloud structure as well as the grain alignment mechanism and its efficiency (e.g., Whittet et al. 2008; Hildebrand et al. 1999). However, this spectrum is only sparsely sampled and further data are needed to better characterize the shape of the spectrum and how it changes across different physical environments.

2. Magnetic Fields

2.1. Galactic-Scale Fields

The polarization of background starlight at optical wavelengths towards thousands of stars has done an excellent job of tracing large-scale magnetic fields in the Galaxy (e.g., Mathewson & Ford 1970; Heiles 2000; Berdyugin, Pirola, & Teerikorpi 2004). These observations trace the field only in diffuse regions of the ISM where optical photons can penetrate ($A_V < \text{few magnitudes}$). The inferred field is in general parallel to the Galactic plane. However, in denser regions of the ISM as traced by FIR–SMM polarimetry it is unclear whether there exists such a correlation with the Galactic plane (e.g., Hildebrand 2001; Li et al. 2006; Vaillancourt 2007).

Further information on the Galactic magnetic field comes from MM-wave observations intended to study Galactic emission as a foreground contaminant to the cosmic microwave background (CMB). An all-sky survey at 94 GHz ($\lambda = 3.2 \text{ mm}$) performed by the WMAP satellite finds a mean magnetic field parallel to the plane (Kogut et al. 2007; Page et al. 2007; Hinshaw et al. 2008), in good agreement with optical polarimetry. WMAP’s spatial resolution for polarization detections at 94 GHz is poor ($\sim 4^\circ$) compared to other existing optical and FIR–SMM observations. For this reason, and the fact that its long wavelength is more sensitive to colder dust, WMAP is likely sampling much more of the magnetic field in the diffuse ISM than are shorter wavelength FIR–SMM observations. That is, it is sampling more of the dust also seen at optical wavelengths than in the FIR–SMM. Future CMB polarization experiments will have increased spatial resolution (\sim several arcminutes) and extend to wavelengths as short as $850 \mu\text{m}$ (Takahashi et al. 2008; Tauber 2004; Aumont 2008).

2.2. Intermediate Scales

At the smallest angular scales gravitational collapse, turbulent motions, and other effects are likely to distort the magnetic field direction with respect to any regularity that may be imposed upon it by the larger ambient Galactic field. A number of authors have tried to compare the field direction inferred from starlight polarization with that from SMM polarimetry. The success has been limited due to the very few locations where such a comparison can be undertaken, and the difficulty of estimating and removing foreground polarization from the starlight measurements (Schleuning et al. 2000; Schleuning 1998; Li et al. 2006; Poidevin & Bastien 2006; Poidevin 2008).

The limited sensitivity of the current generation of SMM polarimeters does not allow magnetic fields to be mapped with high spatial resolution towards precisely the same areas as existing starlight polarization data in diffuse areas of the ISM. However, sensitivity to low-surface brightness clouds can be in-

creased by either binning maps made at high-spatial resolution, or designing an instrument with intrinsically large beams. Such measurements can be compared to higher resolution observations to investigate how the magnetic field structure changes across multiple cloud scales. For example, in the Galactic center, SMM polarimetry on degree scales ($5'$ resolution) reveals a toroidal field, parallel to the plane (Novak et al. 2003). This is in contrast to the existence of non-thermal (synchrotron emitting) filaments with long axes perpendicular to the Galactic plane (Yusef-Zadeh, Morris, & Chance 1984; Yusef-Zadeh, Hewitt, & Cotton 2004; Nord et al. 2004), which has been taken as evidence of a poloidal field within 20° of the Galactic center. However, on smaller scales (arcminutes) toroidal fields are observed in the densest clouds but poloidal fields in the less dense regions (Chuss et al. 2003). This apparently discrepant structure has been interpreted as evidence of a globally poloidal Galactic center field which has been sheared into a toroidal field due to rotation of the dense material about the center.

A similar comparison can be made in the filamentary molecular cloud NGC 6334 (Fig. 1). The large-scale magnetic field ($5'$ resolution) is mostly perpendicular to the long axis of the filament. This filament contains 4 dense cores whose polarization has been mapped at higher spatial resolution ($20''$). The field in the cores exhibits clear similarities to the large-scale field at the maximum extent of the high-resolution data but also shows clear deviations from this field as one moves closer to the core centers.

2.3. Cloud and Star Formation

In models of magnetically regulated cloud and star-formation, molecular clouds are divided into two classes (e.g., Mouschovias & Spitzer 1976; Tomisaka et al. 1988). In the supercritical case, the cloud mass is large enough that gravitational collapse can proceed even against the outward force of magnetic pressure. In the subcritical case the magnetic field prevents compression perpendicular to the field lines, and the cloud can only collapse parallel to the field. In this case, one might expect clouds to be flattened parallel to the field.

Observational examples of this geometry include the clouds DR 21 (Fig. 2a; Kirby 2009), OMC-1 (Schleuning 1998), and OMC-3 (Matthews, Wilson, & Fiege 2001). Tassis et al. (in prep.) have studied how the mean projected magnetic field correlates with cloud elongation and polarization position angle using a large collection of 100 and $350 \mu\text{m}$ polarization data (Dotson et al. 2000, 2009). A preliminary analysis suggests that a model in which the field is perpendicular to the long axis of the clouds is favored over other orientations, even when accounting for projection effects. However, other studies suggest that the elongation directions are random with respect to the field direction (Glenn, Walker, & Young 1999). Drawing strong conclusions from the existing work is difficult, as these data sets are limited to fewer than 20 clouds and few have large aspect ratios.

The magnetic pressure that maintains subcritical clouds can do so only by acting on charged particles. As a result, dense cores may evolve from a subcritical to supercritical state as neutrals diffuse through the field (ambipolar diffusion). The subsequent gravitational collapse pulls the field along, resulting in the classical “hour-glass” field morphology (e.g. Shu, Adams, & Lizano 1987;

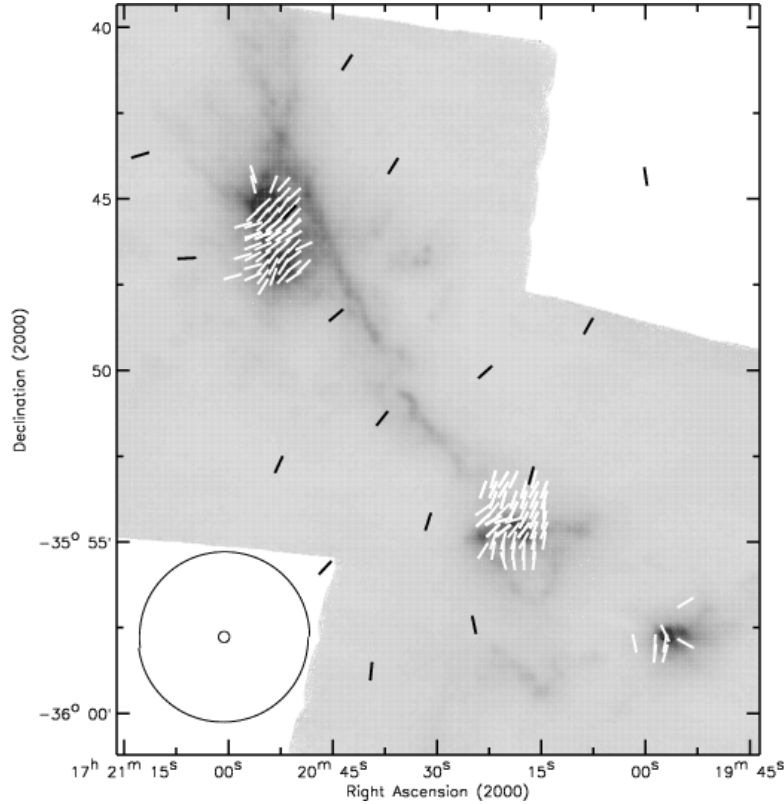


Figure 1. The position angle direction of the magnetic field in NGC 6334 is inferred from polarization observations at $350\ \mu\text{m}$ (white vectors; Dotson et al. 2009) and $450\ \mu\text{m}$ (black vectors; Li et al. 2006). The circles at lower-right show the relative beam sizes of the polarization measurements ($350\ \mu\text{m} = 20''$; $450\ \mu\text{m} = 5''$). The grayscale intensity was obtained with the $350\ \mu\text{m}$ camera SHARC-II at the Caltech Submillimeter Observatory. The intensity is shown with a logarithmic-stretch and has a spatial resolution of $10''$ (courtesy C. D. Dowell).

Vallée 2003). “Pinched” fields in OMC-1 (Schleuning 1998), DR 21 Main (Fig. 2*b*; Kirby 2009), and NGC 1333 IRAS 4A (Girart, Rao, & Marrone 2006) are observational examples of this geometry.

The observations of OMC-1 and NGC 1333 do not cover sufficient spatial extent such that the magnetic field is observed to merge back into the larger-scale Galactic field in which the clouds are embedded. However, in the case of DR21 Main, Kirby (2009) has argued that the orientation of magnetic field vectors support a model in which the central portions of the cloud are undergoing gravitational collapse, but the outer portions of the cloud are supported by magnetic pressure, retaining the field direction in the ambient ISM. Figure 2*b* shows $350\ \mu\text{m}$ intensity and polarization maps of this cloud. By estimating the cloud mass and magnetic field strength as a function of distance from the core, Kirby (2009) finds that the gravitational and magnetic energies are balanced at a distance of approximately 1 pc from the central core. As a result the cloud

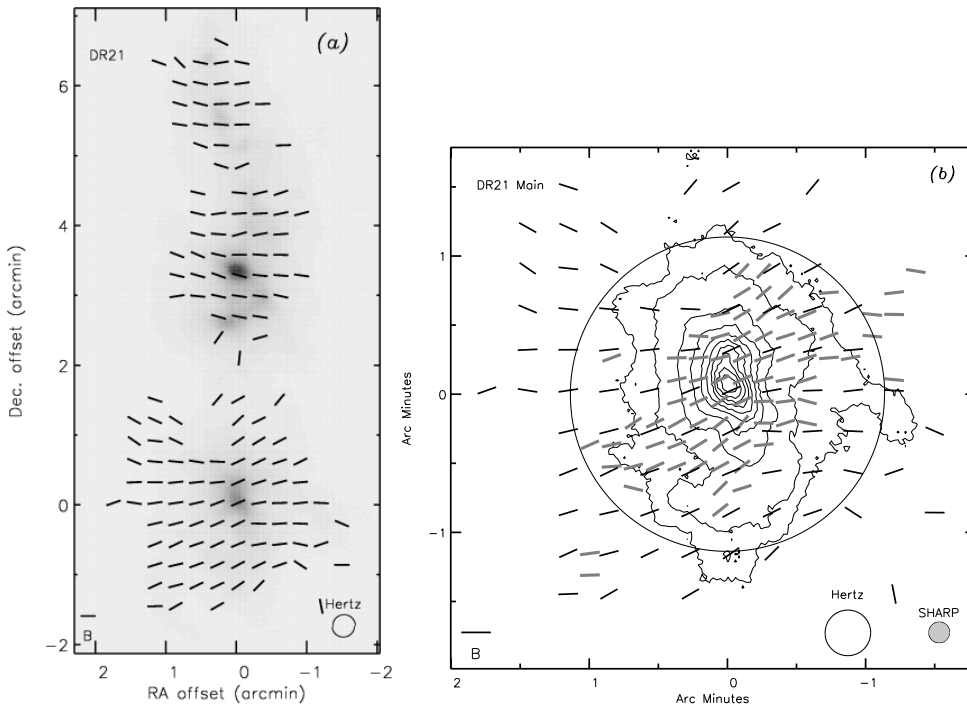


Figure 2. Flux and polarization maps of DR 21 at $350\ \mu\text{m}$ (Kirby 2009). (a) Inferred magnetic field direction in the DR 21 filament at $20''$ resolution (Dotson et al. 2009). North-to-south this map includes the cores DR21 OH FIR2, DR21 OH, and DR21 Main. (b) DR21 Main only, with data from both Hertz (black vectors) and SHARP ($10''$ resolution; gray vectors). The large circle has a radius of 1 pc and indicates the distance from the core beyond which the cloud is prevented from undergoing gravitational collapse due to magnetic pressure; the cloud should collapse only within the circle. Intensity maps from SHARC-2 (courtesy C. D. Dowell).

is expected to collapse gravitational on smaller scales, but remain supported at larger scales. This is consistent with the observation that the magnetic field vectors are more nearly parallel to the ambient field (traced by the filament in Fig. 2a) at the larger scales.

To further test theories of magnetically regulated star and cloud formation polarization maps need to be extended into lower column density regions of these clouds. For example, while the observation of NGC 1333 IRAS 4A (Girart et al. 2006) has excellent spatial resolution ($\sim 1''$) the measurements do not clearly connect to the larger-scale ambient medium (the interferometric measurements are not sensitive to the more extended emission). Thus these polarization measurements will need to be supplemented by single dish measurements (e.g., Li et al. 2008; Bastien et al. 2008) in order to connect such small- and intermediate-scale observations.

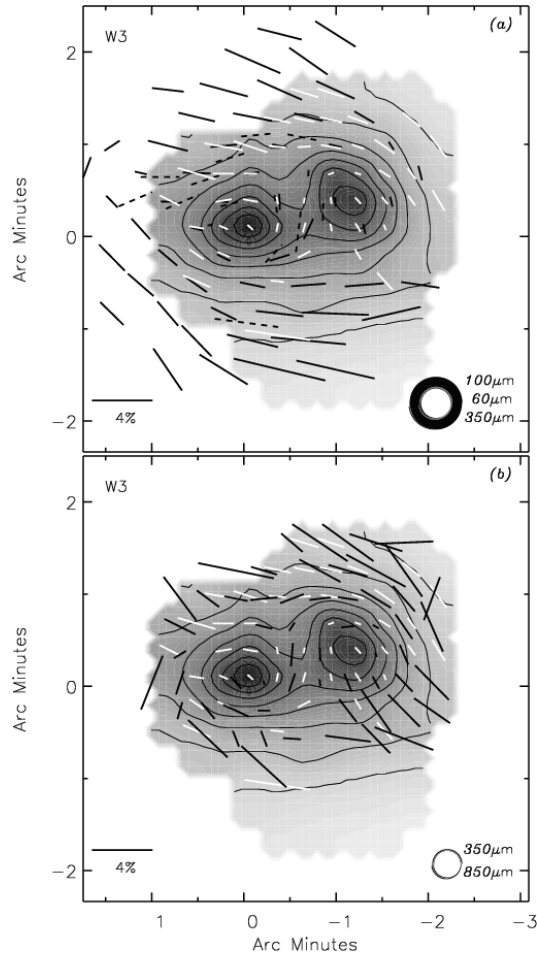


Figure 3. Multiwavelength polarization vectors in the W3 molecular cloud overlaid on 350 μm intensity grayscale and contours. (a) 60 μm (dashed-black vectors with 22'' resolution), 100 μm (solid-black; 35''), and 350 μm (solid-white; 20''). (b) 350 μm (solid-white vectors with 20'' resolution) and 850 μm (solid-black; 18''). The 350 μm polarization and intensity data in (a) and (b) are from the same dataset (Dotson et al. 2009). The 60 and 100 μm data are from Dotson et al. (2000) and the 850 μm data are from Matthews et al. (2008).

3. Polarization Spectra

3.1. Empirical Results

At visible wavelengths, much has been inferred about dust grain physical properties from spectropolarimetry (e.g., Whittet et al. 2001, 2008; Whittet 2004, 2008; Hildebrand & Dragovan 1995). For example, we know that large grains (radii $> 0.1 \mu\text{m}$) are more efficient polarizers than small grains (radii $< 0.01 \mu\text{m}$), silicate grains are better aligned than graphite grains, and the shape of aligned grains is more oblate (disc-like) than prolate (needle-like).

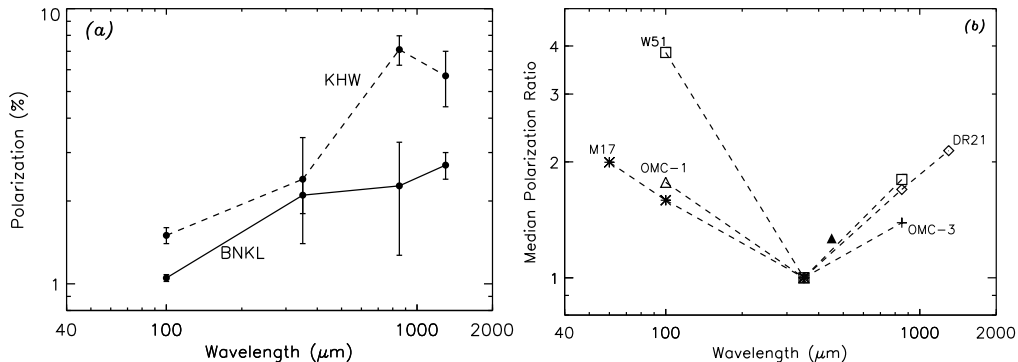


Figure 4. FIR–MM polarization spectra in Galactic molecular clouds. (a) Two separate cloud cores in the Orion Molecular Cloud (data from Schleuning 1998 and Coppin et al. 2000). (b) Cloud “envelopes” (away from dense cores) in several different clouds (Vaillancourt et al. 2008). Envelope polarizations have been normalized at 350 μm within each cloud. The solid triangle at 450 μm is from the data shown in Figure 5b.

Observations of FIR–MM polarimetry have generated polarization maps which span wavelengths of 60 – 1300 μm . Figure 3 shows one such example in the W3 molecular cloud where data are available at 60, 100, 350, and 850 μm . The position angle shows little-to-no change with wavelength in the outer portions of the cloud. However, in the inner regions, position angle changes are clearly evident. Such changes with wavelength indicate the existence of both a changing magnetic field, as well as changes in the dust emission properties, along the line-of-sight through the cloud (Schleuning et al. 2000).

Changes in the polarization *amplitude* with wavelength are also observed in the FIR–MM (e.g., Hildebrand et al. 1999; Vaillancourt 2002, 2007). In the densest cores of molecular clouds the spectrum increases with wavelength (Fig. 4a). In this case, the rise is consistent with an opacity effect (Schleuning 1998). As the opacity increases towards shorter wavelengths the emitted polarization must decrease, approaching zero as the emission becomes optically thick.

In cloud envelopes, where the emission is typically optically thin, the spectrum falls with wavelength below 350 μm , but rises at longer wavelengths (Fig. 4b). This behavior is not consistent with a simple isothermal dust model but requires multiple grain populations where each population’s polarization efficiency is correlated with either the dust temperature or spectral index (Hildebrand et al. 1999; Vaillancourt 2007).

The measured polarization spectrum is sparsely sampled in terms of the number of wavelengths and has not been measured in very many clouds. The goal of current observations is to better populate this spectrum. Vaillancourt & Matthews (2008) have compared the polarization in 15 clouds at wavelengths of 350 and 850 μm . A preliminary analysis is consistent with the results of Figure 4b in which $P(850) > P(350)$ in each of these clouds. Vaillancourt et al. (2008) have also begun a campaign to map the 350-to-450 μm polarization ratio in the same set of Galactic clouds. Results in the Orion Molecular Cloud (Fig. 5) show that the $P(450)/P(350)$ ratio varies across the cloud. The ratio is less than unity towards the SMM intensity peak of the Kleinmann-Low nebula. However,

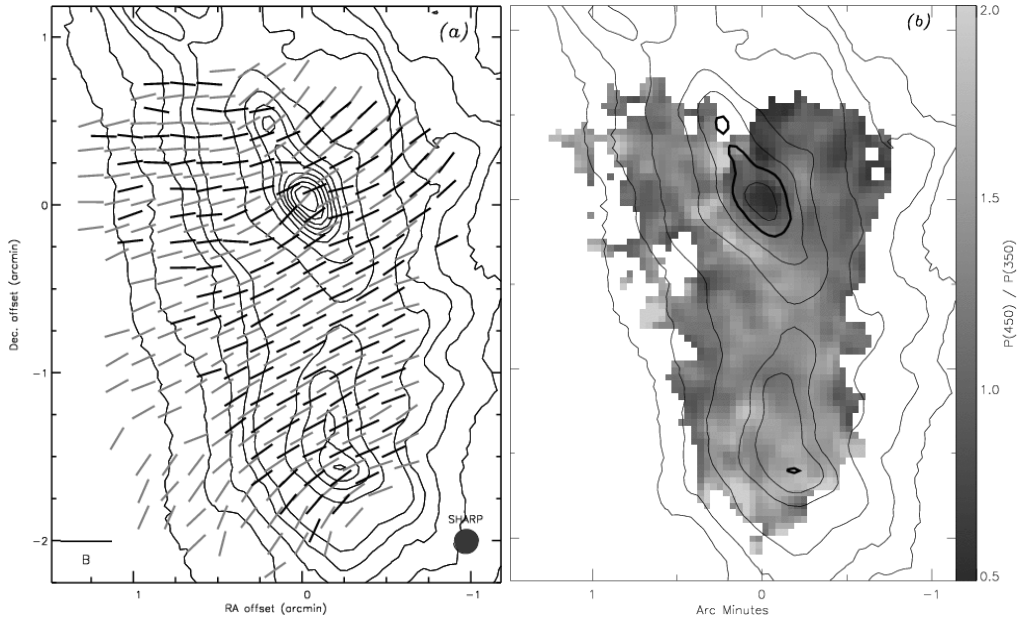


Figure 5. Multi-wavelength polarimetry of the Orion Molecular Cloud (OMC-1) from the SHARP polarimeter (Vaillancourt et al. 2008). The 350 μm intensity peak (contours) at the coordinate origin is towards the Kleinmann-Low nebula. (a) 350 (gray) and 450 (black) μm inferred magnetic field vectors. These vectors are drawn at a constant length that is not proportional to the polarization amplitude. (b) The grayscale indicates the ratio of the 450-to-350 μm polarization amplitudes.

in the cloud envelope outside of this core the ratio is larger, with a median of $P(450)/P(350) = 1.3$; this is consistent with the previous measurements in other clouds shown in Figure 4b.

3.2. Cloud and Dust Models

The rising polarization spectrum at $\lambda > 350 \mu\text{m}$ can be reproduced with a model in which the colder grains are better aligned than the warmer grains. That is, for a two component model we require temperatures $T_A > T_B$ and polarizations $p_A < p_B$. Bethell et al. (2007) have shown that this can be achieved by applying the radiative torque model of grain alignment (e.g., Draine & Weingartner 1996, 1997) to starless clouds. In their model the cloud structure is “clumpy” (or fractal) such that external photons can penetrate deep into the cloud. These photons heat all grains, but the larger grains tend to be cooler as they are more efficient emitters. At the same time, the alignment mechanism is more efficient at aligning the larger grains (Cho & Lazarian 2005). Therefore, this model predicts that the cooler grains are better aligned and that the polarization spectrum rises with wavelength.

While the Bethell et al. (2007) model predicts the qualitative behavior in part of the observed polarization spectra, it does not predict the fall in polarization with wavelength for $\lambda < 350 \mu\text{m}$. Additionally, their predicted spectrum rises by a factor of a few from 100 to 500 μm while the observed spectra rise

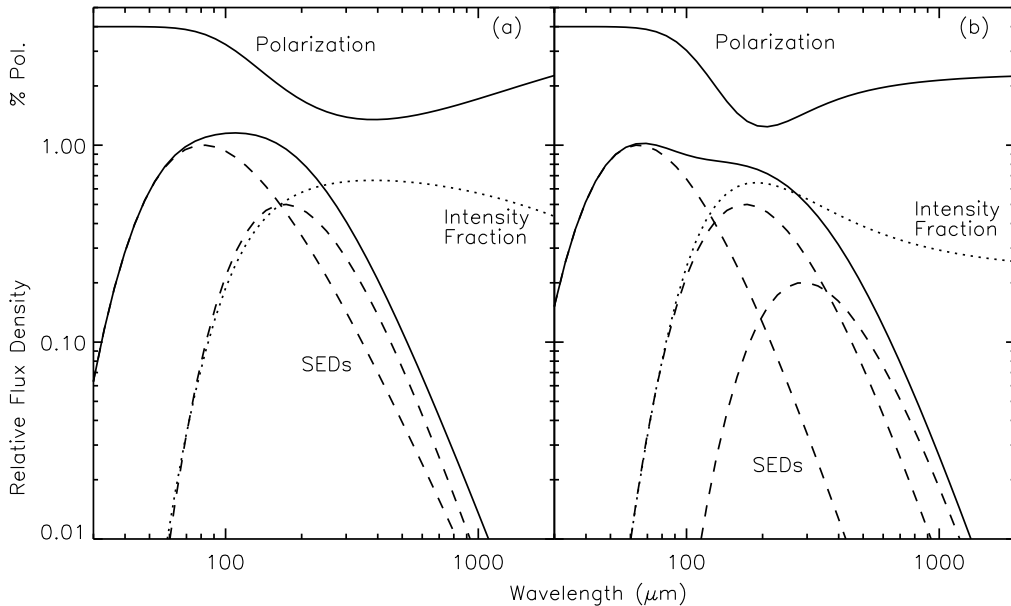


Figure 6. Example SEDs and predicted polarization spectra. Solid lines show the total emission or polarization from the individual components drawn as dashed lines. Dotted lines show the relative contribution to the total intensity of the unpolarized components; the cold component in (a) or the intermediate temperature component in (b). (a) A two-temperature component SED with $T_{1,2} = 45$ and 17 K; $p_{1,2} = 4$ and 0 %; and $\beta_{1,2} = 1$ and 2 , respectively. (b) A three-temperature component SED with $T_{1,2,3} = 45$, 17 , and 10 K; $p_{1,2,3} = 4$, 0 , and 3 %, respectively; and $\beta_{1,2,3} = 2$ for all components.

within the range $350 - 1300 \mu\text{m}$. In real molecular clouds there exist embedded stars that provide an additional source of photons, which will both heat and align dust grains. One can expect that grains closer to these stars will be warmer and better aligned than grains that are either further from stars or shielded from photons in optically thick clumps. This naturally produces grain populations in which the warmer grains are better aligned. The result is a polarization spectrum that falls with wavelength. The observed polarization spectrum with a minimum between 100 and $850 \mu\text{m}$ can in fact be modeled by incorporating embedded stars into the models of starless cores (A. Lazarian, private communication).

3.3. Observational Tests: The Spectral Energy Distribution

If multiple temperatures or spectral indices exist along the line of sight in molecular clouds, as predicted by the model of the polarization spectrum, then one expects this to have an observable effect on the total intensity spectral energy distribution (SED). Unfortunately, little data exist in the clouds and wavelength range ($\lambda \sim 50 - 1000 \mu\text{m}$) of interest to perform definitive tests using measurements of both the polarization spectrum and SEDs. Vaillancourt (2002) found that existing SEDs in the OMC-1 molecular cloud were consistent with the mul-

multiple temperature hypothesis. However, the SEDs were sparsely sampled (maps of the region were available at only 6 wavelengths from 60 to 1100 μm) and the flux uncertainties were large (calibration uncertainties as large as 30%). As a result it was difficult to distinguish between fits to one-temperature component models vs. two-temperature component models.

Consider the multi-component SEDs in Figure 6. The intensity of each component i , at frequency ν , is given by $I_\nu(T_i) = N_i \nu^{\beta_i} B_\nu(T_i)$, where N_i is the column density of each component. The polarization spectrum is high at wavelengths where the total intensity is dominated by a warm polarized component and low at wavelengths dominated by an unpolarized component. In the two-component model with different spectral indices (Fig. 6a) a polarization minimum occurs because the polarized component dominates at both short and long wavelengths, but not intermediate wavelengths. In the three-component model with equal spectral indices (Fig. 6b) the polarization minimum occurs because the intermediate temperature is unpolarized while the colder and warmer components are both polarized. The latter model is similar to the Bethell et al. (2007) model but with the addition of embedded stars.

From these models we see that the wavelength of the polarization minimum is dependent only on the spectral shape of the components and independent of both the relative column densities N_i and polarization efficiencies p_i . For example, as any temperature T_i is changed the corresponding normalized SED will simply shift along the wavelength axis, changing the location at which it contributes its maximum to the total intensity. One could also shift the curves in intensity by changing the relative amounts of cold and warm dust. However, such intensity shifts will only change the absolute and relative values of the polarization, not its spectral shape. As a result, one could use the polarization spectrum to further constrain models of the SED (Hildebrand & Kirby 2004).

3.4. Observational Tests: Embedded Stars

Another test of the polarization spectrum model is to directly compare the locations of embedded stars in molecular clouds with the measured polarization amplitude. If photons are required for efficient grain alignment (e.g., Draine & Weingartner 1997) then one should find increased alignment efficiency (and therefore increased polarization) near embedded stars when compared to nearby locations without stars. While embedded stars are readily found using near-infrared imaging, such comparisons are difficult. For example, Figure 7 compares 3.6 μm emission (mostly stellar) and 350 μm emission (cold dust) in the W3 molecular cloud. The 20'' resolution (typical in the SMM) of the 350 μm observations is insufficient to resolve individual stars due to the relatively high stellar density. Also shown is the 10'' beam of the SHARP polarimeter, which is capable of resolving individual stars in the outer regions of the map.

FIR instruments with higher spatial resolution ($\sim 5''$; Vaillancourt et al. 2007; Dowell et al. 2003) will likely be needed for a more unambiguous comparison in the densest regions. FIR observations will also be more sensitive to the warm dust near these embedded stars, perhaps providing a larger contrast between the cold and warm dust in these regions. For example, Schleuning et al. (2000) have shown that 60 μm polarization observations towards a radio H II region in W3 show a clear increase as opposed to much lower polarization away

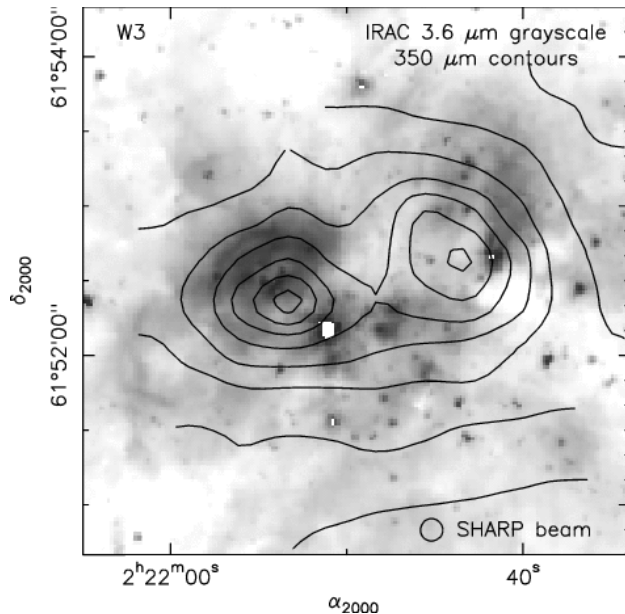


Figure 7. The W3 molecular cloud at $3.6\ \mu\text{m}$ from *Spitzer/IRAC* (grayscale; courtesy C. D. Dowell) and $350\ \mu\text{m}$ from Hertz (contours; Schleuning et al. 2000). The $350\ \mu\text{m}$ intensity and polarization measurements in Figure 3, with a $20''$ spatial resolution, are unable to resolve individual stars; future polarimeters with better spatial resolution ($10''$; Li et al. 2008; Vaillancourt et al. 2007) are expected to do so.

from the H II region. This same trend is not obvious at $350\ \mu\text{m}$ towards the same feature.

4. Summary

The increasingly large database of far-infrared and submillimeter polarimetry is just beginning to allow studies of interstellar magnetic fields across a wide range of size scales. Future polarization measurements with interferometers, such as the Submillimeter Array (Marrone & Rao 2008) and ALMA¹ (Tarengi 2008), will continue to sample star-forming regions on arc-second scales. Single-dish observations (e.g., Li et al. 2008; Bastien et al. 2008) will be required to detect the extended emission from nascent molecular clouds and connect the smallest-scale fields to intermediate scales. Mapping magnetic fields on the larger scales (several arc-minutes – several degrees) requires large beams which must necessarily sacrifice spatial resolution (e.g., Novak et al. 2003; Li et al. 2006). Current large-scale (sub-)millimeter surveys designed to measure the polarization of the cosmic microwave background (e.g., Page et al. 2007; Takahashi et al. 2008) on degree-scale sizes are too large to perform direct comparisons with the existing arc-minute scale observations. However, future survey experiments such as the

¹<http://www.alma.nrao.edu/>

Planck satellite (Tauber 2004; Aumont 2008) are expected to reach resolutions of a few arcminutes.

The existing data also allow for further studies of the dependence of the polarization amplitude on wavelength. The observed spectrum with a polarization minimum near $\lambda \sim 350 \mu\text{m}$ can be understood if there exist correlations between the polarization and either the dust temperature or emissivity. Such correlations are expected to occur naturally in molecular clouds given realistic simulations (Bethell et al. 2007) which incorporate modern grain alignment theory (e.g., Lazarian 2007).

However, the data in both polarization and total intensity are too sparse to provide quantitative tests of the polarization spectrum models. Therefore, our immediate goal is to collect more data in terms of increased wavelength coverage, different types of cloud environments (temperatures and densities), and increased spatial resolution. Future work in all these areas will continue to come from a number of submillimeter instruments on both single-dish telescopes and interferometric arrays. Data in the far-infrared will also provide both increased spatial resolution and access to shorter wavelengths. These wavelengths are crucial to further test and characterize the polarization spectrum and will require far-infrared instruments on airborne or space-based observatories.

Acknowledgments. I would like to thank the conference organizers for inviting me to present this work. Many collaborators have contributed to this work over the years, including Roger Hildebrand, Darren Dowell, Larry Kirby, Giles Novak, Martin Houde, Michael Attard, Hua-bai Li, Megan Krejny, Jessie Dotson, Jackie Davidson, Brenda Matthews, and Hiroko Shinnaga. The author has received support from the U.S. National Science Foundation award AST 05-40882 to the California Institute of Technology.

References

- Aumont, J. 2008, in this volume
 Bastien, P., et al. 2008, in this volume
 Berdyugin, A., Piirola, V., & Teerikorpi, P. 2004, *A&A*, 424, 873
 Bethell, T. J., Chepurnov, A., Lazarian, A., & Kim, J. 2007, *ApJ*, 663, 1055
 Cho, J. & Lazarian, A. 2005, *ApJ*, 631, 361
 Chuss, D. T., Davidson, J. A., Dotson, J. L., Dowell, C. D., Hildebrand, R. H., Novak, G., & Vaillancourt, J. E. 2003, *ApJ*, 599, 1116
 Coppin, K. E. K., Greaves, J. S., Jenness, T., & Holland, W. S. 2000, *A&A*, 356, 1031
 Dotson, J. L., Davidson, J., Dowell, C. D., Schleuning, D. A., & Hildebrand, R. H. 2000, *ApJS*, 128, 335
 Dotson, J. L., Davidson, J. A., Dowell, C. D., Hildebrand, R. H., Kirby, L., & Vaillancourt, J. E. 2008, *ApJS*, submitted
 Dowell, C. D., Davidson, J. A., Dotson, J. L., Hildebrand, R. H., Novak, G., Rennick, T. S., & Vaillancourt, J. E. 2003, in *Proc. SPIE 4843, Polarimetry in Astronomy*, ed. S. Fineschi (SPIE), 250
 Draine, B. T. & Weingartner, J. C. 1996, *ApJ*, 470, 551
 —. 1997, *ApJ*, 480, 633
 Girart, J. M., Rao, R., & Marrone, D. P. 2006, *Science*, 313, 812
 Glenn, J., Walker, C. K., & Young, E. T. 1999, *ApJ*, 511, 812
 Heiles, C. 2000, *AJ*, 119, 923
 Hildebrand, R. & Kirby, L. 2004, in *ASP Conf. Ser. 309, Astrophysics of Dust*, ed. A. N. Witt, G. C. Clayton, & B. T. Draine (San Francisco: ASP), 515

- Hildebrand, R. H. 2001, in *Astrophysical Spectropolarimetry*, ed. J. Trujillo-Bueno, F. Moreno-Insertis, & F. Sanchez (Cambridge: Cambridge University Press), 265
- Hildebrand, R. H., Dotson, J. L., Dowell, C. D., Schleuning, D. A., & Vaillancourt, J. E. 1999, *ApJ*, 516, 834
- Hildebrand, R. H. & Dragovan, M. 1995, *ApJ*, 450, 663
- Hinshaw, G., et al. 2009, *ApJS*, 180, 225
- Kirby, L. 2009, *ApJ*, 694, 1056
- Kogut, A., et al. 2007, *ApJ*, 665, 355
- Lazarian, A. 2007, *J. Quant. Spectros. Radiat. Transfer*, 106, 225
- Li, H., Dowell, C. D., Kirby, L., Novak, G., & Vaillancourt, J. E. 2008, *Appl. Optics*, 47, 422
- Li, H., Griffin, G. S., Krejny, M., Novak, G., Loewenstein, R. F., Newcomb, M. G., Calisse, P. G., & Chuss, D. T. 2006, *ApJ*, 648, 340
- Marrone, D. P. & Rao, R. 2008, in *Proc. SPIE 7020, Millimeter and Submillimeter Detectors and Instrumentation*, ed. W. D. Duncan, W. S. Holland, S. Withington, & J. Zmuidzinas, 7020-2B
- Mathewson, D. S. & Ford, V. L. 1970, *MmRAS*, 74, 139
- Matthews, B. C., McPhee, C., Fissel, L., & Curran, R. 2009, *ApJS*, in press.
- Matthews, B. C., Wilson, C. D., & Fiege, J. D. 2001, *ApJ*, 562, 400
- Mouschovias, T. C. & Spitzer, Jr., L. 1976, *ApJ*, 210, 326
- Nord, M. E., Lazio, T. J. W., Kassim, N. E., Hyman, S. D., LaRosa, T. N., Brogan, C. L., & Duric, N. 2004, *AJ*, 128, 1646
- Novak, G., et al. 2003, *ApJ*, 583, L83
- Page, L., et al. 2007, *ApJS*, 170, 335
- Poidevin, F. 2008, in this volume
- Poidevin, F. & Bastien, P. 2006, *ApJ*, 650, 945
- Schleuning, D. A. 1998, *ApJ*, 493, 811
- Schleuning, D. A., Vaillancourt, J. E., Hildebrand, R. H., Dowell, C. D., Novak, G., Dotson, J. L., & Davidson, J. A. 2000, *ApJ*, 535, 913
- Shu, F. H., Adams, F. C., & Lizano, S. 1987, *ARA&A*, 25, 23
- Takahashi, Y. D., et al. 2008, in *Proc. SPIE 7020, Millimeter and Submillimeter Detectors and Instrumentation*, ed. W. D. Duncan, W. S. Holland, S. Withington, & J. Zmuidzinas, 7020-1D
- Tarengi, M. 2008, *Ap&SS*, 313, 1
- Tauber, J. A. 2004, in *The Magnetized Interstellar Medium*, ed. B. Uyaniker, W. Reich, & R. Wielebinski, 191
- Tomisaka, K., Ikeuchi, S., & Nakamura, T. 1988, *ApJ*, 326, 208
- Vaillancourt, J. E. 2002, *ApJS*, 142, 53
- Vaillancourt, J. E. 2007, in *EAS Publ. Ser. 23, Sky Polarisation at far-infrared to radio wavelengths: The Galactic Screen before the Cosmic Microwave Background*, ed. F. Boulanger & M.-A. Miville-Deschênes (EDP Sciences), 147
- Vaillancourt, J. E., et al. 2007, in *Proc. SPIE 6678, Infrared Spaceborne Remote Sensing and Instrumentation XV*, ed. M. Strojnik, 6678-0D
- Vaillancourt, J. E., et al. 2008, *ApJ*, 679, L25
- Vaillancourt, J. E. & Matthews, B. C. 2008, in this volume
- Vallée, J. P. 2003, *New Astronomy Review*, 47, 85
- Whittet, D. 2008, in this volume
- Whittet, D. C. B. 2004, in *ASP Conf. Ser. 309, Astrophysics of Dust*, ed. A. N. Witt, G. C. Clayton, & B. T. Draine (San Francisco: ASP), 65
- Whittet, D. C. B., Gerakines, P. A., Hough, J. H., & Shenoy, S. S. 2001, *ApJ*, 547, 872
- Whittet, D. C. B., Hough, J. H., Lazarian, A., & Hoang, T. 2008, *ApJ*, 674, 304
- Yusef-Zadeh, F., Hewitt, J. W., & Cotton, W. 2004, *ApJS*, 155, 421
- Yusef-Zadeh, F., Morris, M., & Chance, D. 1984, *Nat*, 310, 557